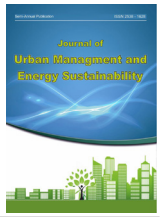
International Journal of Urban Management and Energy Sustainability (IJUMES)

Homepage: http://www.ijumes.com



CASE STUDY RESEARCH PAPER

Numerical Analysis of Raft Foundation Behavior on Soils with Subsurface Voids Using PLAXIS 3D

Gholam Moradi[1*], Mortatha Qasim[2]

1 Department of Civil Engineering, University of Tabriz, Tabriz, Iran

2 Department of Geotechnical Engineering, University of Tabriz, Tabriz, Iran

ARTICLE INFO

Article History:
Received 2026-02-02
Revised 2026-04-09
Accepted 2026-05-15

Keywords:
Bearing-capacity ratio; Cavity interaction; Differential settlement; Hardening Soil model; Three-dimensional finite-element analysis

ABSTRACT

Subsurface voids such as karst cavities, abandoned qanats, and old mine workings interrupt stress transfer beneath shallow foundations and can cause bearing-capacity loss, excessive settlement, and structural rotation. Most previous studies, however, have examined strip or isolated footings, plane-strain conditions, single cavities, or ultimate capacity alone, so the three-dimensional response of finite rafts remains poorly understood. This study aims to quantify how cavity size, depth, horizontal offset, shape, number, and spacing govern the ultimate and serviceability performance of a raft foundation. A 10 m × 15 m reinforced-concrete raft on homogeneous silty sand was modeled in PLAXIS 3D with the Hardening Soil model, and one no-void reference model and 22 voided models were analyzed under identical conditions. Reliability was confirmed through mesh-convergence and boundary-sensitivity analyses, analytical and equilibrium checks, and reconstruction of a published laboratory test. The reference raft reached an ultimate bearing pressure of 2,795 kPa and settled 19.4 mm at 250 kPa. Increasing D/B from 0.10 to 0.40 reduced the bearing-capacity ratio from 0.907 to 0.542 and increased settlement by up to 141%, whereas increasing H/B from 0.25 to 1.50 raised BCR from 0.624 to 0.984, with cavity influence becoming negligible at H/B = 1.00. The critical horizontal offset occurred at X/B = 0.50, which produced the largest differential settlement and tilt, and three closely spaced cavities reduced BCR to 0.565. Because capacity, settlement, and rotation were governed by different configurations, cavity-affected rafts should be assessed against both ultimate and serviceability criteria.

DOI: 10.22034/ijumes.2026.2108969.1424

Running Title: Raft Foundation Behavior on Soils

NUMBER OF REFERENCES 26

NUMBER OF FIGURES 03

NUMBER OF TABLES 02

*Corresponding Author:
Email: *gmoradi@tabrizu.ac.ir*
Phone: 00989375120607
ORCID: https://orcid.org/0000-0002-7881-2039

INTRODUCTION

Subsurface voids constitute a significant source of uncertainty in foundation engineering because they interrupt the continuity of the load-bearing ground while frequently remaining undetected during routine site investigation. Such openings may originate from karst dissolution, internal erosion, abandoned qanats, old mines, utility tunnels, wells, pipelines, or poorly backfilled excavations. Urban expansion increases the likelihood that new buildings will be constructed above or near these features. When structural loading is applied, the soil roof over a void may deform, yield, or collapse, producing abrupt settlement and damage to the supported structure. The problem becomes more complex when two or more openings interact within the same influence zone. Recent analyses of footings above dual tunnels have shown that tunnel arrangement, spacing, ground strength, and load inclination jointly govern bearing resistance and the geometry of the failure mechanism (Huang et al., 2026). A subsurface cavity changes the natural path through which foundation stresses spread into the ground. Part of the load is redirected around the cavity crown and sidewalls, creating stress concentration and reducing the effective soil volume available for resistance. The resulting response depends on cavity size, cover depth, horizontal position, shape, and the mechanical properties of the surrounding material. A shallow or large cavity can connect directly with the foundation failure zone, whereas a sufficiently deep cavity may have only a limited effect. Dynamic conditions introduce additional complexity because inertial forces modify stress orientation and mobilized resistance. Seismic finite-element limit analyses have demonstrated that cavity geometry and horizontal acceleration must be assessed simultaneously when estimating bearing-capacity reduction, rather than applying independent correction factors to an intact-ground solution (Xiao et al., 2025). Raft foundations are commonly selected when structural loads are high, soil resistance is limited, or differential settlement must be controlled. Their large contact area and flexural stiffness permit load redistribution and partial bridging over locally weakened ground. However, the same large plan dimensions increase the probability that a concealed cavity will occur below an edge, corner, or interior region of the raft. A centered void may cause nearly symmetric settlement, while an eccentric void can generate unequal contact pressure, differential settlement, bending, twisting, and rotation. Importantly, the most unfavorable position is not necessarily beneath the raft center because stress transfer is influenced by the relationship between cavity location and raft edges. Laboratory testing of eccentrically loaded footings above single voids confirms that load eccentricity and cavity position interact in controlling settlement, rotation, and progressive failure (Wu et al., 2025). Conventional bearing-capacity equations generally assume a continuous soil mass and cannot explicitly reproduce stress bypass, cavity-roof deformation, or interaction between separate openings. Numerical modeling is therefore required to represent the cavity as an actual geometric discontinuity and trace changes in stress, displacement, contact pressure, and plasticity throughout loading. Three-dimensional analysis is particularly necessary for a finite raft and isolated cavities because two-dimensional plane-strain models represent openings as infinitely long tunnels and suppress load transfer around their ends. Rigid-plastic finite-element studies have established that cavity depth, size, shape, and horizontal distance define distinct influence zones and failure mechanisms (Keba Lukueta & Isobe, 2024). Nevertheless, many published investigations remain focused on strip or isolated footings, two-dimensional conditions, ultimate bearing capacity alone, or single-cavity configurations. The present study addresses these limitations through a controlled three-dimensional parametric investigation of a reinforced-concrete raft over unsupported subsurface cavities using PLAXIS 3D. A verified no-void model provides the reference response, after

which normalized cavity size, clear-cover depth, horizontal offset, number, spacing, and shape are varied systematically. Performance is evaluated using ultimate bearing pressure, bearing-capacity ratio, total and differential settlement, raft tilt, contact-pressure redistribution, cavity-roof displacement, and plastic-zone connectivity. The novelty of the study lies in combining ultimate and serviceability criteria within one consistent framework and in identifying critical configurations for both single and interacting cavities. Unlike studies that rank scenarios solely by collapse pressure, this investigation distinguishes symmetric capacity loss from asymmetric serviceability damage. It also maintains identical soil, raft, interface, boundary, mesh, and loading conditions across every model to permit defensible comparisons. Previous three-dimensional research has confirmed that foundation shape and cavity eccentricity materially affect bearing resistance, supporting the need for spatial modeling (Khosravi et al., 2024). The resulting thresholds are intended for preliminary risk assessment, not as universal design limits, and indicate when detailed investigation, cavity treatment, ground improvement, or foundation relocation is warranted.

MATERIALS AND METHODS

Numerical research has shown that cavities reduce the resistance available beneath shallow foundations by interrupting the development of the conventional shear zone. Alzabeebee et al. (2024) used two-dimensional finite-element analysis to investigate the undrained bearing-capacity factor of a strip footing above a cavity and subsequently developed an evolutionary polynomial regression equation. Their analyses reported reductions ranging from 3% to 79%, depending on cavity dimensions and position. Increasing cavity depth or horizontal distance generally reduced the adverse effect, while shallow openings located within the principal failure zone produced substantial capacity loss and altered the governing mechanism. Adaptive finite-element limit analysis has provided upper- and lower-bound estimates for foundations influenced by multiple openings. P. Kumar and Chauhan (2024a) examined a footing above dual circular cavities in a rock mass and demonstrated that cavity spacing, depth, and relative position control whether the openings behave independently or form a combined failure mechanism. Closely spaced cavities generated interacting plastic zones and greater capacity reductions, whereas increasing their separation progressively restored the response toward that of a single opening. Their findings emphasize that the number of cavities cannot be represented adequately by multiplying the effect obtained for one isolated cavity.

Cavity shape is a governing parameter because it controls stress concentration and the orientation of yielding around an underground opening. A. Kumar, Chauhan, Kumar, et al. (2024) compared tunnel geometries beneath shallow foundations and showed that openings with sharp corners or extended roofs can generate failure patterns different from those associated with circular configurations. Even when openings have comparable dimensions, the distribution of unsupported material and curvature affects stress bypass, plastic-zone development, and ultimate resistance. Consequently, design conclusions obtained for circular tunnels should not be transferred directly to rectangular, square, or horseshoe-shaped cavities without an explicit geometric assessment. External loading conditions can modify foundation–tunnel interaction. P. Kumar et al. (2024) investigated shallow foundation behavior near tunnels under complex loading and found that vertical, horizontal, inclined, and eccentric load components change both the magnitude of resistance and the direction of the failure mechanism. Under nonvertical loading, stress concentration becomes asymmetric and the critical tunnel location may shift relative to the footing centerline. These results indicate that cavity position cannot be assessed independently of load direction, particularly for structures subjected to lateral forces, overturning

moments, machinery loads, wind actions, or seismic demand. The computational cost of extensive parametric analyses has encouraged the integration of numerical methods with data-driven prediction. A. Kumar, Chauhan, and Kumar (2024) combined adaptive finite-element limit analysis with artificial neural networks and multiple linear regression to estimate the stability of a shallow foundation above a horseshoe tunnel. Their work demonstrated that trained surrogate models can reproduce multidimensional numerical trends efficiently and identify the relative importance of geometric and rock-mass parameters. Nevertheless, surrogate predictions remain dependent on the range, quality, and mechanical consistency of the numerical database used for training, and they cannot replace verification of the original model. Experimental studies remain necessary because they reveal deformation patterns and reinforcement effects that may not be captured by an idealized numerical formulation. Kazemzadeh et al. (2024) examined a foundation on geogrid-reinforced sand containing twin subsurface voids. Their results showed that reinforcement improved load distribution and limited settlement by transferring tensile forces across weakened regions, while the response remained sensitive to void arrangement and soil compaction. This work also highlighted the distinction between studying the untreated foundation–void mechanism and evaluating a mitigation system, because reinforcement may change both the magnitude and spatial distribution of failure.

Serviceability behavior has received less attention than ultimate resistance, despite the possibility that settlement may become unacceptable before collapse. Shubham et al. (2024) generated a PLAXIS 2D database and developed a shallow neural-network surrogate for predicting foundation settlement above a circular cavity within a reliability framework. Their study incorporated uncertainty in input parameters and demonstrated that probabilistic settlement assessment can provide information that deterministic capacity calculations overlook. However, two-dimensional settlement models cannot reproduce finite-cavity end effects, biaxial raft bending, plan rotation, or spatial interaction among several three-dimensional openings. Wu et al. (2024) studied strip footings above tunnels under inclined loading using finite-element limit analysis. Their upper- and lower-bound solutions differed by less than 3%, providing stable estimates of ultimate capacity and failure envelopes. The results showed that load inclination and tunnel geometry jointly affect bearing resistance and failure-pattern evolution. Increasing the horizontal component reduced the available vertical capacity and redirected the plastic mechanism toward the tunnel. Such findings reinforce the need to define loading assumptions explicitly and show why results obtained under centered vertical pressure represent a controlled baseline rather than every field loading condition. Load eccentricity becomes particularly important when more than one cavity is present. P. Kumar and Chauhan (2024b) evaluated eccentrically loaded strip footings above dual cavities using adaptive upper- and lower-bound limit analysis. They considered different arrangements of circular openings and demonstrated that footing eccentricity, cavity spacing, depth, and alignment interact in determining the stability number. Symmetric cavity layouts did not necessarily produce symmetric mechanisms when the load was eccentric. Their recommendations therefore relied on normalized geometric and loading parameters, illustrating that a single critical-distance rule cannot describe all multiple-cavity configurations. Xiao et al. (2023) investigated strip footings above rectangular voids in Hoek–Brown rock masses and produced dimensionless reduction charts based on adaptive upper-bound finite-element limit analysis. Their results confirmed that void width, height, vertical cover, horizontal distance, geological strength index, intact strength, and material constant influence capacity and failure geometry. Collectively, previous studies establish the importance of cavity geometry and loading,

but most address strip or isolated footings, plane-strain openings, rock masses, ultimate resistance, or one variable group. A gap therefore remains for verified three-dimensional analysis of a finite raft that simultaneously compares size, depth, offset, shape, number, and spacing using both ultimate and serviceability indicators.

Methodology

Numerical Research Design

This study adopted a quantitative, numerical, and controlled parametric design to evaluate the response of a finite raft foundation located above subsurface cavities. Three-dimensional finite-element analyses were performed using PLAXIS 3D because the finite dimensions of both the raft and the cavities allow stress redistribution around all sides of each opening. The numerical program comprised one no-void reference model and 22 distinct models containing subsurface cavities. The reference model established the baseline ultimate bearing capacity, settlement, contact-pressure distribution, and failure mechanism. In the subsequent analyses, one group of geometric parameters was varied at a time, while the soil properties, raft characteristics, soil–raft interface, groundwater conditions, model boundaries, mesh configuration, and loading procedure were kept unchanged. Previous finite-element limit analyses of eccentrically loaded foundations above parallel tunnels have demonstrated the importance of controlling cavity geometry and loading position when comparing different subsurface configurations (Zhang et al., 2023).

Each simulation followed the same sequence: generation of the soil domain and raft geometry, assignment of material properties, calculation of the initial stress state, creation of the cavity or cavities, activation of the raft and interface elements, staged application of pressure, extraction of numerical responses, and comparison with the no-void reference model. Ultimate-limit-state and serviceability-limit-state responses were evaluated separately. This distinction prevented a configuration with adequate collapse resistance but unacceptable settlement or rotation from being classified as satisfactory. All numerical outputs were recorded at identical prescribed loading increments to ensure consistent comparisons among the models.

Model Geometry and Dimensionless Parameters

The reference foundation consisted of a rectangular reinforced-concrete raft with a width of B = 10 m, a length of L = 15 m, and a uniform thickness of t = 0.50 m. The raft was positioned at the ground surface and centered within a soil domain measuring 60 × 60 × 40 m, corresponding to 6B × 6B × 4B. These dimensions provided sufficient lateral and vertical clearance between the foundation, cavities, and model boundaries and were subsequently evaluated through a boundary-sensitivity analysis. The primary opening was represented as an unsupported spherical cavity with diameter D. The clear-cover depth H was measured vertically from the underside of the raft to the crown of the cavity. The horizontal offset X was defined as the horizontal distance between the centerline of the raft and the centerline of the cavity. In the multiple-cavity configurations, S represented the center-to-center spacing between adjacent cavities. Accordingly, the principal dimensionless parameters were defined as D/B, H/B, X/B, and S/B. Studies of eccentrically loaded footings above circular cavities have demonstrated that normalized cavity size, vertical distance, horizontal offset, and loading position govern the reduction in bearing capacity and the development of failure mechanisms (P. Kumar & Chauhan, 2023). The cavity-size series covered D/B = 0.10–0.40, whereas the depth series included H/B = 0.25–1.50. The horizontal-offset series covered X/B = 0–1.00, and the double- and triple-cavity models included spacing ratios of S/B = 0.30–1.00.

Spherical, cubical, and vertical cylindrical cavities with equal volumes were also compared to isolate the effect of cavity shape. For each model, the depth of the cavity center, zc, was calculated

as follows:

$$zc = H + D/2$$

Twin cavities were positioned symmetrically relative to the raft centerline. The triple-cavity arrangement consisted of one central cavity and two lateral cavities. Before analysis, all configurations were checked to prevent cavity overlap and intersection with the raft, ground surface, or model boundaries. (Fig. 1)

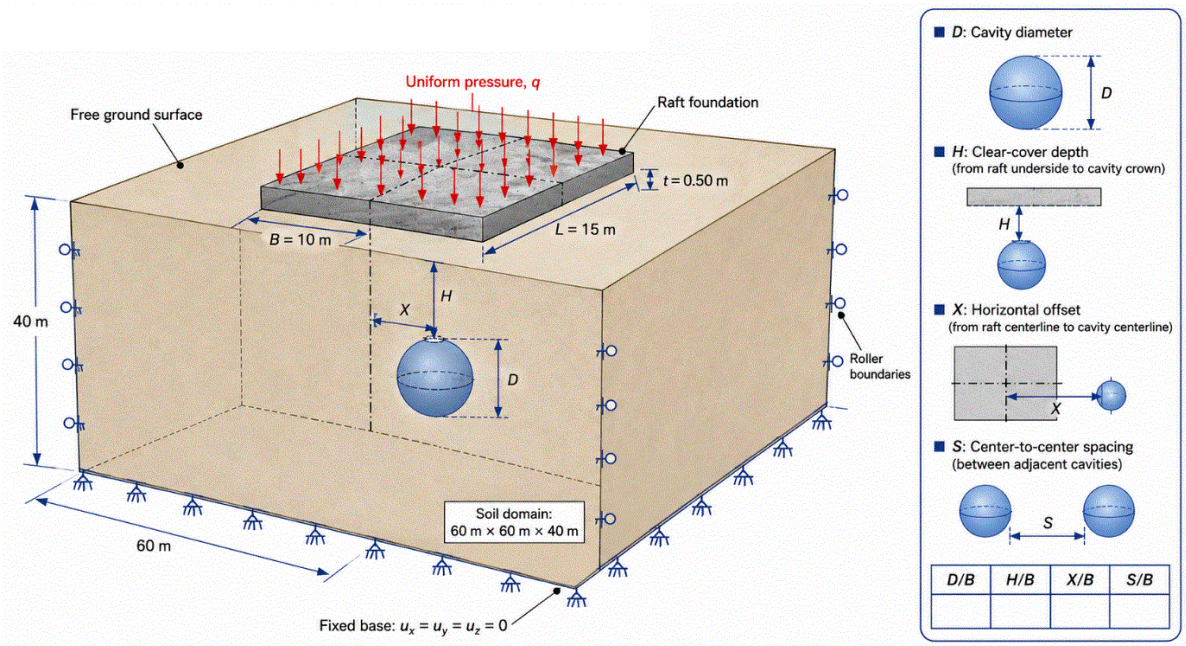


Figure 1: Three-dimensional geometry, boundary conditions, and definitions of the normalized parameters D/B, H/B, X/B, and S/B for the raft–soil–void model.

Material Properties and Soil–Raft Interface

The soil was idealized as homogeneous medium-dense silty sand to isolate the influence of cavity geometry from the effects of soil stratification. The Hardening Soil model (Schanz et al., 1999) was adopted as the principal constitutive model because it accounts for stress-dependent stiffness and distinguishes among primary loading, oedometer loading, and unloading–reloading responses. The unsaturated and saturated unit weights of the soil were γ_{ansat} = 18 kN/m³ and γ_{sat} = 20 kN/m³, respectively. The effective cohesion, effective friction angle, and dilatancy angle were c' = 5 kPa, φ' = 32°, and ψ = 2°, respectively. The reference secant stiffness, reference oedometer stiffness, and reference unloading–reloading stiffness were E_{50}^{raf} = 30,000 kPa, E_{oed}^{ref} = 30,000 kPa, and Ec = 90,000 kPa, respectively. The stress-dependency exponent was m = 0.50, the unloading–reloading Poisson's ratio was ν_{ur} = 0.20, and the failure ratio was Rf = 0.90. The soil deposit was considered normally consolidated, with an overconsolidation ratio of OCR = 1.00 and an initial lateral earth-pressure coefficient of K_0 = 0.47. The hydraulic conductivity was k = 0.10 m/day, and the groundwater table was located 20 m below the ground surface. Drained conditions were assigned because the cavities were situated above the groundwater table and the applied loading was monotonic. The raft was represented as an isotropic linear-elastic plate. The concrete unit weight was γc = 25 kN/m³, Young's modulus was Ec = 30,000,000 kPa, and Poisson's ratio was νc = 0.20. A zero-thickness soil–raft interface with a strength-reduction factor of R_{inter} = 0.80 was introduced to permit compression, shear transfer,

relative slip, and possible separation without imposing artificial bonding. The cavity surfaces were modeled as unsupported and traction-free, while the raft remained elastic throughout all calculation phases.

No random spatial variability was introduced into the soil properties. Limit-analysis investigations of footings above circular voids have similarly shown that soil strength parameters and normalized cavity geometry must be defined consistently to obtain reliable comparisons (Chauhan et al., 2023). The adopted material properties and numerical-model parameters are summarized in (Tab. 1).

Table 1: Material properties, raft characteristics, and numerical-model parameters

Component	Parameter	Symbol	Value	Unit
Soil	Soil type	—	Medium-dense silty sand	–
	Constitutive model	—	Hardening Soil	–
	Drainage condition	—	Drained	–
	Unsaturated unit weight	γ_{unsat}	18	kN/m³
	Saturated unit weight	γ_{sat}	20	kN/m³
	Effective cohesion	c'	5	kPa
	Effective friction angle	φ'	32	degree
	Dilatancy angle	ψ	2	degree
	Secant stiffness	E_{50ref}	30,000	kPa
	Oedometer stiffness	E_{oedref}	30,000	kPa
	Unloading–reloading stiffness	E_{urref}	90,000	kPa
	Stress-dependency exponent	m	0.50	–
	Unloading–reloading Poisson's ratio	ν_{ur}	0.20	–
	Failure ratio	R_f	0.90	–
	Hydraulic conductivity	k	0.10	m/day
	Overconsolidation ratio	OCR	1.00	–
	Initial lateral-pressure coefficient	K_0	0.47	–
Groundwater	Water-table depth	—	20	m
Raft	Width	B	10	m
	Length	L	15	m
	Thickness	t	0.50	m
	Concrete unit weight	γ_c	25	kN/m³
	Young's modulus	E_c	30,000,000	kPa
	Poisson's ratio	ν_c	0.20	–
Interface	Strength-reduction factor	R_{inter}	0.80	–
Model	Soil-domain dimensions	—	60 × 60 × 40	m
Loading	Maximum applied pressure	q_{max}	3,500	kPa

Boundary Conditions, Mesh, and Loading

The bottom boundary of the soil domain was fixed against displacement in all three directions. The vertical boundaries normal to the x-axis were restrained against horizontal displacement in the x-direction ($u_x = 0$), while the boundaries normal to the y-axis were restrained against displacement in the y-direction ($u_y = 0$). Vertical

displacement was permitted along the lateral boundaries. The ground surface remained free except at the raft–soil contact, and all cavity surfaces were unsupported and traction-free. The soil domain was discretized using ten-node quadratic tetrahedral elements. The raft was represented using six-node plate elements, together with compatible interface elements along the raft–soil contact. A medium global mesh was combined with local refinement beneath the raft, along the raft edges, around the cavity surfaces, and within the soil bridges separating adjacent cavities. The selected mesh comprised approximately 142,000 soil elements and 204,000 nodes. Experimental and numerical investigations of footings near subsurface cavities have demonstrated that mesh-convergence evaluation and comparison of load–settlement responses are necessary for credible interpretation of numerical results (Azeddine & Abdelghani, 2023). Initial stresses were generated using the K_0 procedure. The cavities were subsequently created, after which the raft and interface elements were activated. Displacements were reset before the application of external loading.

A uniformly distributed vertical pressure was increased from zero to q_{max} = 3,500 kPa through staged drained calculations. The ultimate bearing pressure, q_{ult}, was determined using the first applicable criterion among a distinct peak in the pressure–settlement curve, uncontrolled deformation or numerical nonconvergence associated with failure, and attainment of a normalized settlement of:

$$s/B = 0.10$$

Smaller automatic load substeps were permitted near sharp changes in the pressure–settlement curve or the onset of convergence difficulties. Identical prescribed pressure increments were used for all primary geometric configurations to ensure direct comparison of capacity, settlement, differential settlement, and raft rotation.

Verification and Validation

Verification and validation were treated as complementary but distinct components of the numerical assessment. Verification examined whether the adopted discretization, domain dimensions, and numerical calculations provided stable solutions, whereas validation evaluated the ability of the model to reproduce independently observed foundation behavior.

Mesh convergence was assessed using coarse, selected, and fine discretizations. For the no-void model NV-00, the corresponding ultimate bearing pressures were 2,860, 2,795, and 2,768 kPa. The settlements calculated at an applied pressure of q = 250 kPa were 18.6, 19.4, and 19.8 mm, respectively. The percentage differences between the selected and fine meshes were calculated as:

$$\text{Capacity difference} = |2{,}795 - 2{,}768|/2{,}768 \times 100 = 0.98\%$$

$$\text{Settlement difference} = |19.4 - 19.8|/19.8 \times 100 = 2.02\%$$

For the single-void model SV-00, the corresponding differences between the selected and fine meshes were 0.99% for ultimate capacity and 1.77% for settlement. These differences satisfied the predefined acceptance limits of 2% for bearing capacity and 3% for deformation. Therefore, the selected mesh was adopted because it provided an appropriate balance between numerical accuracy and computational demand. Boundary sensitivity was examined by comparing the standard domain of 6B × 6B × 4B with an enlarged domain of 8B × 8B × 5B. The resulting ultimate-capacity differences were 0.54%, 0.67%, and 0.96% for models NV-00, SV-00, and TV-S30, respectively. Differences in settlement remained below 1.52% for all three configurations. Furthermore, the computed plastic zones did not extend to the restrained model boundaries, indicating that the selected domain dimensions did not artificially constrain the failure mechanisms. The ultimate bearing pressure obtained from the no-void Hardening Soil model was q_{ult} = 2,795 kPa.

This value was within the analytical interval of 2,620–2,910 kPa and differed by only 1.09% from the midpoint of that interval. The result therefore provided an additional check on the general magnitude of the numerical bearing capacity.

Global vertical equilibrium was assessed by integrating the contact pressure acting beneath the raft. At an applied pressure of q = 250 kPa, the total vertical action, including the self-weight of the raft, was 39,375 kN. The calculated resultant of the raft contact pressure was 39,108 kN. The equilibrium imbalance was consequently:

Equilibrium imbalance = |39,375 − 39,108|/39,375 × 100 = 0.68%

The imbalance remained below 1% at higher loading stages, confirming acceptable numerical force equilibrium.

External validation was performed by reconstructing a published strip-footing experiment involving a circular subsurface void. At normalized settlements of s/B = 1%, 2%, 4%, 6%, 8%, and 10%, the measured pressures were 55, 95, 150, 180, 198, and 210 kPa, respectively. The corresponding numerical pressures were 58, 92, 146, 176, 203, and 216 kPa. The mean absolute error was calculated as:

$$MAE = (1/n)\,\Sigma|q_{num} - q_{exp}| = 4.17\ kPa$$

The mean absolute percentage error was:

$$MAPE = (100/n)\,\Sigma|(q_{num} - q_{exp})/q_{exp}| = 3.15\%$$

The difference between the experimental and numerical ultimate pressures was 2.86%. These results indicate that the model reproduced both the general shape and magnitude of the experimental pressure–settlement response with acceptable accuracy.

Constitutive-model sensitivity was also examined. Relative to the Hardening Soil model, the Mohr–Coulomb model predicted 4.1–9.8% greater ultimate bearing capacity and 9.3–12.7% smaller service-level settlement. This discrepancy was interpreted as constitutive-model uncertainty rather than discretization error. The Hardening Soil model was therefore retained for all primary analyses because it more realistically represents stress-dependent soil stiffness and hardening behavior.

Figure 2 presents the mesh-convergence and experimental-validation curves. Overall, the mesh, boundary, equilibrium, analytical, experimental, and constitutive checks satisfied the predefined acceptance criteria. The selected three-dimensional numerical model was consequently considered sufficiently reliable for the subsequent parametric analyses. (Fig. 2)

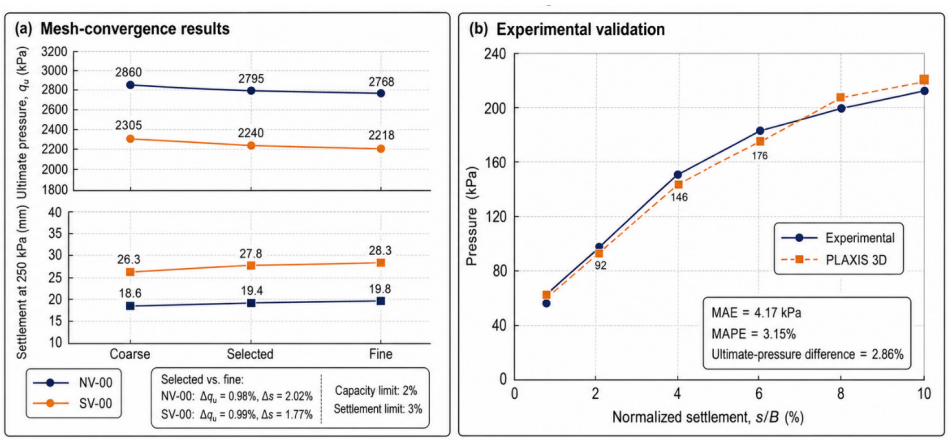


Figure 2: Mesh-convergence and experimental-validation curves used to assess the reliability of the numerical model.

FINDINGS AND DISCUSSION

Reference No-Void Response

Model NV-00 established the intact-ground reference for all normalized comparisons. Its pressure–settlement response remained approximately linear up to an applied pressure of 500 kPa and became progressively nonlinear as yielding expanded beneath the raft edges. At the service pressure of q = 250 kPa, the maximum and minimum settlements were 19.4 and 18.1 mm, respectively. The resulting differential settlement was:

$$\Delta s = s_{max} - s_{min} = 19.4 - 18.1 = 1.3 \text{ mm}$$

Raft tilt was negligible under the service load. The ultimate bearing pressure was q_{ult} = 2,795 kPa at the adopted normalized-settlement criterion of s/B = 0.10. Accordingly, the bearing-capacity ratio of the reference model was:

$$BCR = q_{ult,voi}d/q_{ult,no\text{-}voi}d = 1.000$$

At q = 250 kPa, contact pressure ranged from approximately 218 kPa in the central region to 312 kPa near the raft edges. The integrated contact force remained consistent with the applied vertical resultant. Numerical studies of footings over layered ground containing voids similarly employ an intact-ground configuration to quantify cavity-induced reductions in bearing capacity (Chaabani et al., 2023). No persistent tensile separation developed beneath the raft during the loading stages. Plastic points first appeared beneath the raft edges at approximately 700 kPa and subsequently propagated downward and inward. At the ultimate condition, the plastic zones formed a continuous three-dimensional general-shear mechanism. This mechanism remained separated from the lateral and bottom boundaries of the numerical domain. The stable response of NV-00 therefore provided a consistent reference for evaluating all models containing subsurface cavities.

Effect of Void Size and Shape

Void size produced a strong and nonlinear deterioration in raft-foundation performance. For the centered spherical cavity with H/B = 0.50 and X/B = 0, increasing D/B from 0.10 to 0.40 reduced the ultimate bearing pressure from 2,535 to 1,515 kPa. The corresponding bearing-capacity ratios were:

D/B = 0.10: q_{ult} = 2,535 kPa and BCR = 0.907
D/B = 0.20: q_{ult} = 2,240 kPa and BCR = 0.801
D/B = 0.30: q_{ult} = 1,878 kPa and BCR = 0.672
D/B = 0.40: q_{ult} = 1,515 kPa and BCR = 0.542

At the service pressure of q = 250 kPa, the maximum raft settlement increased from 23.1 mm at D/B = 0.10 to 27.8, 35.4, and 46.8 mm at D/B = 0.20, 0.30, and 0.40, respectively. Relative to the no-void settlement of 19.4 mm, these values represented increases of 19.1%, 43.3%, 82.5%, and 141.2%, respectively. The settlement amplification was calculated using:

$$\text{Settlement increase } (\%) = [(s_{voi}d - s_{no\text{-}voi}d)/s_{no\text{-}voi}d] \times 100$$

Because all cavities in this series were centered beneath the raft, differential settlement remained limited and overall raft tilt was negligible. Similar numerical investigations of strip footings in sandy soil have confirmed that cavity dimensions and position control bearing capacity and define a critical zone of influence (Benbouza et al., 2023).

As cavity diameter increased, the unsupported central zone forced contact stresses to redistribute toward the raft perimeter. At D/B = 0.40, the service-level contact pressure reached approximately 428 kPa near the raft edges but decreased to about 124 kPa directly above the cavity center. Plastic yielding initially developed around the cavity crown and subsequently propagated upward toward the raft. As D/B increased, the plastic zone surrounding the cavity connected with the shear zones beneath the raft edges at progressively lower applied pressures.

The equal-volume cavity-shape comparison

produced ultimate bearing pressures of 2,240, 2,105, and 2,170 kPa for the spherical, cubical, and vertical cylindrical cavities, respectively. The corresponding bearing-capacity ratios were:

Spherical cavity: BCR = 0.801
Cubical cavity: BCR = 0.753
Vertical cylindrical cavity: BCR = 0.776

The associated maximum settlements at q = 250 kPa were 27.8 mm for the spherical cavity, 31.6 mm for the cubical cavity, and 29.7 mm for the vertical cylindrical cavity. Among the three equal-volume shapes, the cubical cavity produced the most unfavorable response. Its flat roof and sharp corners generated localized concentrations of shear strain, whereas the curved surface of the spherical cavity enabled smoother three-dimensional stress transfer around the opening.
Figure 3(a) indicates that service settlement was more sensitive than BCR to moderate increases in cavity size. Consequently, cavity severity should not be assessed solely based on ultimate bearing resistance. A configuration may retain a substantial proportion of its no-void bearing capacity while already producing unacceptable service-level deformation.

Effect of Void Depth
Increasing the clear-cover depth progressively separated the cavity from the principal failure zone beneath the raft. For a centered spherical cavity with D/B = 0.20, the ultimate bearing pressures corresponding to H/B = 0.25, 0.50, 0.75, 1.00, and 1.50 were 1,745, 2,240, 2,515, 2,665, and 2,750 kPa, respectively. The corresponding bearing-capacity ratios were:

H/B = 0.25: BCR = 0.624
H/B = 0.50: BCR = 0.801
H/B = 0.75: BCR = 0.900
H/B = 1.00: BCR = 0.953
H/B = 1.50: BCR = 0.984

At the service pressure of q = 250 kPa, the maximum raft settlement decreased from 38.9 mm at H/B = 0.25 to 27.8, 23.2, 21.2, and 20.0 mm at H/B = 0.50, 0.75, 1.00, and 1.50, respectively. Experimental observations of foundations above cavities in unsaturated sand similarly indicate that deeper cavities provide greater bearing resistance and smaller surface deformation than shallow cavities (Keba & Isobe, 2023). A quantitative negligible-influence criterion was adopted to identify the critical clear-cover ratio. The cavity effect was considered negligible when both of the following requirements were satisfied:

$BCR \geq 0.95$
$s_{void} \leq 1.10 s_{no\text{-}void}$

The model with H/B = 0.75 failed both requirements because its BCR was 0.900 and its settlement was 19.6% greater than that of NV-00. In contrast, the model with H/B = 1.00 satisfied both requirements, with BCR = 0.953 and settlement amplification of 9.3%. Therefore, H/B = 1.00 was identified as the critical clear-cover ratio for the adopted soil, raft, and cavity geometry. At H/B = 1.50, settlement differed from the no-void reference value by only 3.1%.

The improvement associated with increasing cavity depth was asymptotic. Increasing H/B from 0.25 to 0.50 increased BCR by 0.177, whereas increasing H/B from 1.00 to 1.50 increased BCR by only 0.031. Over the same depth range, cavity-roof displacement decreased from 26.4 to 1.8 mm.

At shallow cover, a continuous plastic band developed between the raft underside and the cavity crown before the ultimate load was reached. At greater depths, yielding around the cavity roof remained localized, and the dominant shear mechanism increasingly resembled that of the no-void model. Therefore, the critical depth represents a practical performance threshold rather than the complete disappearance of cavity influence. Figure 3(b) illustrates the progressive convergence of raft behavior toward the intact-ground response as H/B increases.

Effect of Horizontal Offset

Horizontal offset produced a nonmonotonic response because cavity position affected both interruption of the vertical load-transfer path and asymmetry of the supporting soil. For D/B = 0.20 and H/B = 0.50, the ultimate bearing pressures at X/B = 0, 0.25, 0.50, 0.75, and 1.00 were 2,240, 2,075, 1,955, 2,350, and 2,705 kPa, respectively. The corresponding bearing-capacity ratios were:

X/B = 0: BCR = 0.801
X/B = 0.25: BCR = 0.742
X/B = 0.50: BCR = 0.699
X/B = 0.75: BCR = 0.841
X/B = 1.00: BCR = 0.968

The lowest bearing-capacity ratio occurred at X/B = 0.50, where the cavity was positioned near the raft edge rather than directly beneath its center. Limit-analysis research on circular foundations above spherical cavities has similarly demonstrated that normalized cavity position governs the ultimate bearing capacity and geometry of the failure mechanism (Keawsawasvong et al., 2023). At q = 250 kPa, the maximum settlement increased from 27.8 mm for the centered cavity to 32.0 and 36.7 mm at X/B = 0.25 and 0.50, respectively. It subsequently decreased to 27.1 mm at X/B = 0.75 and 20.7 mm at X/B = 1.00. Differential settlement increased from 2.1 mm for the centered cavity to 7.6 mm at X/B = 0.25 and reached its maximum value of 12.4 mm at X/B = 0.50. The corresponding transverse raft tilt reached 0.00096 rad and indicated rotation toward the cavity. The maximum contact pressure at the service load increased from approximately 365 kPa in the centered-cavity model to 468 kPa at X/B = 0.50. Cavity-roof displacement simultaneously increased from 12.9 to 18.7 mm. At X/B = 1.00, differential settlement, raft tilt, and cavity-roof displacement decreased to 2.4 mm, 0.00012 rad, and 2.8 mm, respectively. At the critical offset of X/B = 0.50, the plastic zone around the cavity crown connected with the shear band developing beneath the adjacent raft edge. This interaction created an inclined and asymmetric failure surface and resulted in the simultaneous reduction of bearing capacity and increase in raft rotation. At larger horizontal offsets, the cavity-related and raft-related plastic zones became separated, and the contact-pressure distribution became more uniform. These observations confirm the gradual recovery of foundation behavior toward the no-void condition as the cavity moves beyond the principal influence zone. Figure 3(c) identifies X/B = 0.50 as the critical horizontal offset for the investigated configuration. (Fig. 3)

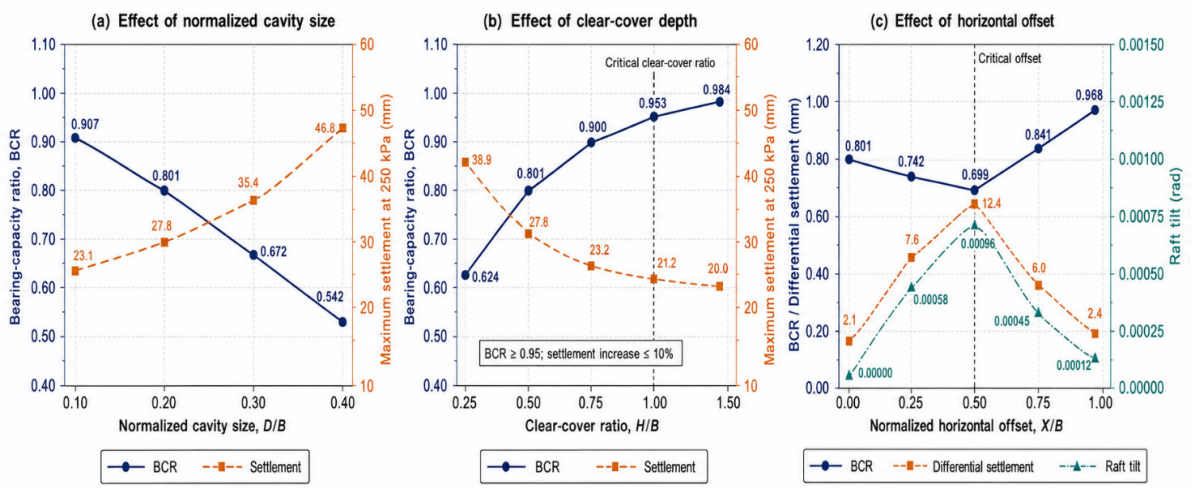


Figure 3: Parametric effects of cavity geometry on raft-foundation performance: (a) effects of normalized cavity size D/B on BCR and settlement; (b) effects of clear-cover ratio H/B on BCR and settlement; and (c) effects of horizontal offset X/B on BCR, differential settlement, and raft tilt.

Effects of Void Number and Spacing

The response of the raft to multiple cavities was investigated using symmetric arrangements of two and three spherical cavities with D/B = 0.20, H/B = 0.50, and spacing ratios ranging from S/B = 0.30 to 1.00. The model containing one centered cavity developed an ultimate bearing pressure of q_u = 2,240 kPa, a bearing-capacity ratio of BCR = 0.801, and a maximum service settlement of 27.8 mm. For the double-cavity configurations, increasing S/B from 0.30 to 1.00 increased the ultimate bearing pressure from 1,860 to 2,140 kPa and raised BCR from 0.665 to 0.766. Over the same spacing range, maximum settlement at the service pressure of q = 250 kPa decreased from 36.8 to 29.8 mm. For the triple-cavity configurations, increasing S/B from 0.30 to 1.00 increased the ultimate bearing pressure from 1,580 to 1,960 kPa. The corresponding BCR increased from 0.565 to 0.701, while maximum service settlement decreased from 42.6 to 33.1 mm. Previous adaptive finite-element analyses have similarly confirmed that normalized cavity dimensions and positions govern the reduction in foundation bearing capacity caused by underground openings (P. Kumar & Chauhan, 2022a). The bearing-capacity ratio was calculated from:

$$BCR = q_{u,voi}d/q_{u,no-voi}d$$

At the smallest spacing ratio of S/B = 0.30, the plastic zones surrounding adjacent cavity crowns overlapped within the intervening soil ligaments. This interaction produced collective yielding beneath the raft and caused the cavities to behave as a weakened group rather than as independent openings. Increasing the spacing progressively separated these plastic zones and allowed distinct stress arches to develop around individual cavities. Nevertheless, the interaction among three cavities remained measurable even at S/B = 1.00.

Because the double- and triple-cavity arrangements were symmetric about the raft centerline, raft tilt remained approximately zero. However, the maximum contact pressure reached 438 kPa in model DV-S30 and 492 kPa in model TV-S30. Therefore, negligible rotation did not necessarily represent acceptable foundation performance.

Model TV-S30 was identified as the critical multiple-cavity configuration because it combined the lowest BCR, the largest total settlement, the greatest cavity-roof displacement, and the most pronounced contact-pressure concentration. These results demonstrate that both cavity number and normalized spacing must be considered when evaluating the performance of foundations above multiple underground openings.

Integrated Quantitative Comparison

Table 2 integrates the principal numerical results and demonstrates that different cavity configurations governed different foundation-performance indicators. Model NV-00 provided the intact-ground reference, with an ultimate bearing pressure of q_u = 2,795 kPa, BCR = 1.000, and a maximum service settlement of 19.4 mm.

The largest centered cavity, represented by model SV-D40, produced the lowest ultimate bearing capacity within the single-cavity series. Its ultimate bearing pressure was q_u = 1,515 kPa, corresponding to BCR = 0.542. Its maximum settlement of 46.8 mm represented an increase of 141.2% relative to the no-void reference condition. The shallow-cavity model SV-H25 also produced severe deterioration, with BCR = 0.624 and a maximum service settlement of 38.9 mm.

The most unfavorable asymmetric condition was observed in model SV-X50. Although its BCR of 0.699 was greater than that of SV-D40, its differential settlement reached 12.4 mm and its transverse raft tilt reached 0.00096 rad. This configuration therefore governed the rotational and angular-distortion responses.

The closely spaced triple-cavity model TV-S30 developed an ultimate bearing pressure of q_u = 1,580 kPa, BCR = 0.565, and a maximum service settlement of 42.6 mm. It was consequently identified as the governing multiple-cavity in-

teraction case.

The comparisons demonstrate that minimum bearing capacity, maximum total settlement, and maximum angular distortion did not occur in the same model. A capacity-based ranking identified SV-D40 as the most adverse case, an angular-distortion assessment identified SV-X50 as the critical asymmetric case, and an interaction-based assessment identified TV-S30 as the critical multiple-opening configuration.

Consequently, engineering assessment should independently consider ultimate bearing pressure, BCR, maximum settlement, differential settlement, and raft tilt before a cavity configuration is classified as acceptable. Reliance on only one response indicator may conceal another governing failure or serviceability mode. (Tab. 2)

Table 2: Quantitative comparison of the principal numerical scenarios

Model	Geometric condition	q_u (kPa)	BCR	Maximum settlement (mm)	Differential settlement (mm)	Raft tilt (rad)
NV-00	No cavity	2,795	1.000	19.4	1.3	≈ 0
SV-D10	D/B = 0.10	2,535	z	23.1	1.6	≈ 0
SV-D40	D/B = 0.40	1,515	0.542	46.8	3.9	≈ 0
SV-H25	H/B = 0.25	1,745	0.624	38.9	< 2.5	≈ 0
SV-H100	H/B = 1.00	2,665	0.953	21.2	< 2.5	≈ 0
SV-X50	X/B = 0.50	1,955	0.699	36.7	12.4	0.00096
DV-S30	Two cavities; S/B = 0.30	1,860	0.666	36.8	2.3–3.6	≈ 0
TV-S30	Three cavities; S/B = 0.30	1,580	0.565	42.6	2.3–3.6	≈ 0

Note: Settlement-related quantities were evaluated at the service pressure of q = 250 kPa. A raft tilt of approximately zero indicates a geometrically symmetric cavity arrangement.

RESULTS AND CONCLUSION

The results are consistent with previous adaptive limit analyses demonstrating that larger, shallower, and critically positioned cavities reduce foundation resistance by connecting cavity-roof yielding with the failure mechanism developing beneath the foundation. P. Kumar and Chauhan (2022b) identified a critical horizontal distance close to 0.5B and a progressive reduction in cavity influence with increasing depth in rock-based strip-footing models. The present three-dimensional raft analyses similarly identified X/B = 0.50 as the critical horizontal offset. However, the negligible-influence depth was found to be H/B = 1.00 when both capacity and settlement criteria were considered. Differences between the reported threshold values can be attributed to the finite geometry of the raft, the mechanical behavior of silty sand, the use of spherical cavities, the Hardening Soil constitutive model, and the inclusion of serviceability requirements. The numerical failure mechanisms explain the observed trends. Large or shallow cavities shortened the available load-transfer and shear-resistance paths. They consequently promoted an early connection between yielding around the cavity crown and the plastic zones forming beneath the raft edges. This interaction reduced the ultimate bearing pressure and increased the service-level settlement. Eccentrically located cavities redirected the applied load toward the better-supported side of the raft. This asymmetric transfer of stress produced contact-pressure concentration, differential settlement, and raft rotation toward the cavity. The most severe asymmetric response occurred when the cavity crown interacted directly with the shear zone beneath the raft edge.

Closely spaced cavities interacted through the yielding soil ligaments separating the openings. At small S/B values, the overlapping plastic zones caused the cavities to behave collectively as one larger weakened region. As spacing increased,

independent stress arches gradually developed around the individual cavities, reducing—but not necessarily eliminating the interaction effect. For engineering applications, detected subsurface cavities should be characterized according to normalized size, clear-cover depth, horizontal offset, number, and center-to-center spacing before foundation performance is evaluated. Depending on the severity and location of the cavities, appropriate remedial measures may include cavity filling, compaction or grouting of the surrounding soil, ground reinforcement, relocation of the foundation, or modification of raft geometry and stiffness.

The critical ratios identified in this study should be interpreted as preliminary screening values applicable to the adopted numerical conditions. They should not be treated as universal design limits. Site-specific soil parameters, groundwater conditions, cavity geometry, loading characteristics, and structural requirements must be incorporated before the results are used in practical foundation design. This study investigated the three-dimensional behavior of a reinforced-concrete raft foundation above unsupported subsurface cavities using PLAXIS 3D. The numerical program comprised one verified no-void reference model and 22 models containing cavities. All models were analyzed using identical soil properties, raft characteristics, interface conditions, model boundaries, mesh settings, groundwater conditions, and loading procedures.

The reliability of the numerical model was evaluated through mesh-convergence analysis, boundary-sensitivity assessment, analytical comparison, global force-equilibrium checks, constitutive-model sensitivity, and reconstruction of a published foundation–void experiment. The external validation produced a mean absolute percentage error of MAPE = 3.15%, while the differences associated with mesh refinement remained within the predefined acceptance limits. These results supported the use of the selected model for the parametric analyses.

The principal conclusions are as follows:

1.The no-void model developed an ultimate bearing pressure of q_u = 2,795 kPa and a maximum settlement of 19.4 mm at the service pressure of q = 250 kPa. These values provided the reference condition for all normalized comparisons.

2.Cavity size strongly influenced both ultimate resistance and serviceability behavior. Increasing D/B from 0.10 to 0.40 reduced BCR from 0.907 to 0.542 and increased maximum service settlement from 23.1 to 46.8 mm. The largest cavity therefore caused a 45.8% reduction in bearing capacity and a 141.2% increase in settlement relative to the no-void model.

3.Cavity shape affected stress redistribution and strain localization. Among equal-volume openings, the cubical cavity produced the most adverse response, followed by the vertical cylindrical and spherical cavities. The flat roof and sharp corners of the cubical cavity intensified shear-strain concentration, whereas the curved spherical surface promoted smoother three-dimensional stress transfer.

4.Increasing clear-cover depth reduced the influence of the cavity. Increasing H/B from 0.25 to 1.50 raised BCR from 0.624 to 0.984 and reduced service settlement from 38.9 to 20.0 mm. The adopted negligible-influence criteria were:

$BCR \geq 0.95$
Settlement amplification $\leq 10\%$

These two requirements were first satisfied at H/B = 1.00. This value represents a model-specific performance threshold and should not be interpreted as a universal critical depth.

5.Horizontal cavity offset produced a non-monotonic foundation response. The critical position occurred at X/B = 0.50 rather than directly beneath the raft center. At this offset, BCR decreased to 0.699, maximum settlement reached 36.7 mm, differential settlement reached 12.4 mm, and raft tilt reached 0.00096 rad. Therefore, a centered cavity was not the governing configuration for asymmetric deformation.

6.Increasing the number of cavities intensified bearing-capacity reduction and settlement, whereas increasing spacing reduced cavity interaction. At S/B = 0.30, BCR decreased from 0.801 for one cavity to 0.665 for two cavities and 0.565 for three cavities. Closely spaced cavities interacted through their yielding soil bridges and behaved as a combined weakened zone.

7.Different configurations governed different performance criteria. Model SV-D40 governed the total loss of bearing capacity, model SV-X50 governed differential settlement and raft rotation, and model TV-S30 governed multiple-cavity interaction. Therefore, the most adverse configuration cannot be identified using only one response variable.

8.Foundation assessment above cavities should simultaneously consider BCR, total settlement, differential settlement, raft tilt, contact-pressure redistribution, cavity-roof displacement, and plastic-zone connectivity. A model satisfying the bearing-capacity requirement may still experience unacceptable service settlement or angular distortion.

The conclusions of this study are limited to homogeneous medium-dense silty sand, drained monotonic loading, idealized unsupported cavities, a linear-elastic raft, and the adopted ranges of normalized geometry. Soil stratification, spatial variability, irregular cavity surfaces, partial cavity filling, time-dependent behavior, and cyclic or seismic loading were not considered. Future research should investigate layered and spatially variable soil deposits, irregular and partially filled cavities, transient groundwater conditions, eccentric and inclined loading, seismic excitation, and nonlinear raft behavior. Physical model testing and field-scale monitoring are also required to evaluate the proposed numerical thresholds under realistic conditions. Before applying the reported values in engineering practice, site-specific strength and stiffness parameters should be determined, and cavity geometry should be verified using appropriate geophysical or intrusive investigation methods. Comparative analyses should then assess untreated, filled, reinforced, and foundation-relocation alternatives using consistent ultimate-limit-state and serviceability-limit-state criteria.

REFERENCES

Alzabeebee, S., Ismael, B. H., Keawsawasvong, S., & Chavda, J. T. (2024). Finite element and evolutionary polynomial regression analyses of the effect of a cavity on the bearing capacity factor Nc of strip footing. Modeling Earth Systems and Environment, 10(3), 3815–3826. https://doi.org/10.1007/s40808-024-01985-6

Azeddine, B., & Abdelghani, M. (2023). The cavity's effect on the bearing capacity of a shallow footing in reinforced slope sand. Soils and Rocks, 46(1), e2023003622. https://doi.org/10.28927/sr.2023.003622

Benbouza, A., Mansouri, T., & Abbeche, K. (2023). Behavior of strip footing/s above void in sandy soil. Engineering, Technology & Applied Science Research, 13(1), 10039–10044. https://doi.org/10.48084/etasr.5494

Chaabani, W., Remadna, M. S., & Abu-Farsakh, M. (2023). Numerical modeling of the ultimate bearing capacity of strip footings on reinforced sand layer overlying clay with voids. Infrastructures, 8(1), 3. https://doi.org/10.3390/infrastructures8010003

Chauhan, V. B., Kumar, P., & Keawsawasvong, S. (2023). Limit analysis solution for ultimate bearing capacity of footing resting on rock mass with a circular void subjected to line loading. Indian Geotechnical Journal, 53(2), 334–347. https://doi.org/10.1007/s40098-022-00676-2

Huang, Y., Kang, X., Dai, D., & Wu, G. (2026). Bearing capacity of inclined-loaded footings above dual tunnels in rock masses. Scientific Reports, 16, 23565. https://doi.org/10.1038/s41598-026-54298-2

Kazemzadeh, M., Pezeshkian, P., Zad, A., & Yazdi, M. (2024). Behavior of a foundation built on geogrid-reinforced sand in the presence of twin subsurface voids. International Journal of Geosynthetics and Ground Engineering, 10(5), 82. https://doi.org/10.1007/s40891-024-00592-w

Keawsawasvong, S., Lai, V. Q., Thongchom, C., & Van, C. N. (2023). Undrained bearing capacity of circular footing above spherical cavity.

In Computational intelligence methods for green technology and sustainable development (pp. 190–200). Springer. https://doi.org/10.1007/978-3-031-19694-2_17

Keba, E. L., & Isobe, K. (2023). Ultimate bearing capacity of a shallow foundation on unsaturated sandy soil with cavity. In Smart geotechnics for smart societies (pp. 1323–1326). CRC Press. https://doi.org/10.1201/9781003299127-193

Keba Lukueta, E., & Isobe, K. (2024). Bearing capacity of a shallow foundation above the soil with a cavity based on rigid plastic finite element method. Applied Sciences, 14(5), 1975. https://doi.org/10.3390/app14051975

Khosravi, S., Karimpour-Fard, M., Shahnazari, H., Aminpour, M., & Nazem, M. (2024). Undrained bearing capacity of circular and square footings above centric and eccentric three-dimensional cavities. International Journal of Geomechanics, 24(6). https://doi.org/10.1061/IJGNAI.GMENG-8835

Kumar, A., Chauhan, V. B., & Kumar, P. (2024). Integration of AFELA and machine learning for analysis of shallow foundation over horseshoe tunnel in rock mass. Modeling Earth Systems and Environment, 10(1), 651–670. https://doi.org/10.1007/s40808-023-01802-6

Kumar, A., Chauhan, V. B., Kumar, P., Chauhan, A. K., & Singh, P. (2024). Interplay of tunnel geometry and shallow foundation stability in rock: Comparative insights into failure modes. International Journal of Geomechanics, 24(9), 04024185. https://doi.org/10.1061/IJGNAI.GMENG-9815

Kumar, P., & Chauhan, V. B. (2022a). Bearing capacity of strip footing resting above a circular void in the rock mass using adaptive finite element method. Innovative Infrastructure Solutions, 7(1), 72. https://doi.org/10.1007/s41062-021-00666-y

Kumar, P., & Chauhan, V. B. (2022b). Ultimate bearing capacity of a foundation on the rock media due to the presence of a circular void: Design tables, failure mechanism, and recommendations. Arabian Journal of Geosciences, 15, 1345. https://doi.org/10.1007/s12517-022-10620-6

Kumar, P., & Chauhan, V. B. (2023). On the eccentrically loaded strip footing resting over a circular cavity in the rock mass: Adaptive finite-element analysis, observations, and recommendations. International Journal of Geomechanics, 23(2), 04022287. https://doi.org/10.1061/IJGNAI.GMENG-7985

Kumar, P., & Chauhan, V. B. (2024a). Behavior of footing resting above dual circular cavities in a rock mass: Insights from an AFELA study. International Journal of Geomechanics, 24(1), 04023248. https://doi.org/10.1061/IJGNAI.GMENG-9036

Kumar, P., & Chauhan, V. B. (2024b). Observations and recommendations for shallow foundation stability over dual cavities in rock mass under eccentric loading utilizing limit analysis. Arabian Journal for Science and Engineering, 49(4), 5875–5895. https://doi.org/10.1007/s13369-023-08524-y

Kumar, P., Chauhan, V. B., & Kumar, A. (2024). Assessing foundation behaviour under complex loading near tunnels. Journal of Mountain Science, 21(10), 3503–3520. https://doi.org/10.1007/s11629-024-8757-y

Schanz, T., Vermeer, P. A., & Bonnier, P. G. (1999). The hardening soil model: Formulation and verification. In R. B. J. Brinkgreve (Ed.), Beyond 2000 in computational geotechnics: 10 years of PLAXIS International (pp. 281–296). Balkema.

Shubham, K., Metya, S., & Sinha, A. K. (2024). Surrogate model-based prediction of settlement in foundation over cavity for reliability analysis. Transportation Infrastructure Geotechnology, 11(3), 1294–1320. https://doi.org/10.1007/s40515-023-00329-8

Wu, G., Tan, Y., Zeng, J., et al. (2025). Laboratory tests of an eccentrically loaded strip footing above single underlying void. Journal of Building Engineering, 111, 113211. https://www.sciencedirect.com/science/article/pii/S2352710225014482

Wu, G., Zeng, J., Zhang, R., Tan, Y., & Zhang, S. (2024). Effects of inclined loads on strip footings with an underlying tunnel. Advances in Engineering Software, 198, 103783. https://doi.org/10.1016/j.advengsoft.2024.103783

Xiao, Y., Lin, Q., Fang, W., & Zhang, R. (2025). Seismic bearing capacity of strip footing above cavities in rock masses. Soils and Foundations, 65(5), 101681. https://www.sciencedirect.com/

science/article/pii/S0038080625001155
Xiao, Y., Zhang, M., Zhou, Z., Hou, Z., Lv, J., Tang, M., & Zhang, R. (2023). Ultimate bearing capacity of strip footings above rectangular voids in Hoek–Brown rock masses. Computers and Geotechnics, 161, 105589. https://doi.org/10.1016/j.compgeo.2023.105589
Zhang, R., Zhao, H., & Wu, G. (2023). FELA investigation of eccentrically-loaded footing on parallel tunnels constructed in rock masses. Computers and Geotechnics, 153, 105102. https://doi.org/10.1016/j.compgeo.2022.105102

COPYRIGHTS
©2023 The author(s). This is an open access article distributed under the terms of the Creative Commons Attribution (CC BY 4.0), which permits unrestricted use, distribution, and reproduction in any medium, as long as the original authors and source are cited. No permission is required from the authors or the publishers.

HOW TO CITE THIS ARTICLE
Moradi, G. & Qasim, M. (2026). Numerical Analysis of Raft Foundation Behavior on Soils with Subsurface Voids Using PLAXIS 3D. (e743664). International Journal of Urban Management and Energy Sustainability, 7(1), e743664
DOI:10.22034/ijumes.2026.2108969.1424